Fluorine-Terminated Diamond Surfaces as Dense Dipole Lattices: The Electrostatic Origin of Polar Hydrophobicity

Leonhard Mayrhofer,*,[†] Gianpietro Moras,[†] Narasimham Mulakaluri,[†] Srinivasan Rajagopalan,*,[‡] Paul A. Stevens,[‡] and Michael Moseler[†,§]

[†]Fraunhofer IWM, MicroTribology Center µTC, Wöhlerstrasse 11, 79108 Freiburg, Germany
[‡]ExxonMobil Research and Engineering Company, Annandale, New Jersey 08801, United States
[§]University of Freiburg, Physics Department, Hermann-Herder-Strasse 3, 79104 Freiburg, Germany

S *Supporting Information*

ABSTRACT: Despite the pronounced polarity of C−F bonds, many fluorinated carbon compounds are hydrophobic: a controversial phenomenon known as "polar hydrophobicity". Here, its underlying microscopic mechanisms are explored by ab initio calculations of fluorinated and hydrogenated diamond (111) surfaces interacting with single water molecules. Gradient- and van der Waals-corrected density functional theory simulations reveal that "polar hydrophobicity" of the fully fluorinated surfaces is caused by a negligible surface/water electrostatic interaction. The densely packed C−F surface dipoles generate a short-range electric field that decays within the core repulsion zone of the surface and hence vanishes in regions accessible by adsorbates. As a result, water physisorption on fully F-terminated surfaces is weak (adsorption energies E_{ad}

< 0.1 eV) and dominated by van der Waals interactions. Conversely, the near-surface electric field generated by loosely packed dipoles on mixed F/H-terminated surfaces has a considerably longer range, resulting in a stronger water physisorption (E_{ad} > 0.2 eV) that is dominated by electrostatic interactions. The suppression of electrostatic interactions also holds for perfluorinated molecular carbon compounds, thus explaining the prevalent hydrophobicity of fluorocarbons. In general, densely packed polar terminations do not always lead to short-range electric fields. For example, surfaces with substantial electron density spill-out give rise to electric fields with a much slower decay. However, electronic spill-out is limited in F/H-terminated carbon materials. Therefore, our ab initio results can be reproduced and rationalized by a simple classical point-charge model. Consequently, classical force fields can be used to study the wetting of F/H-terminated diamond, revealing a pronounced correlation between adsorption energies of single H_2O molecules and water contact angles.
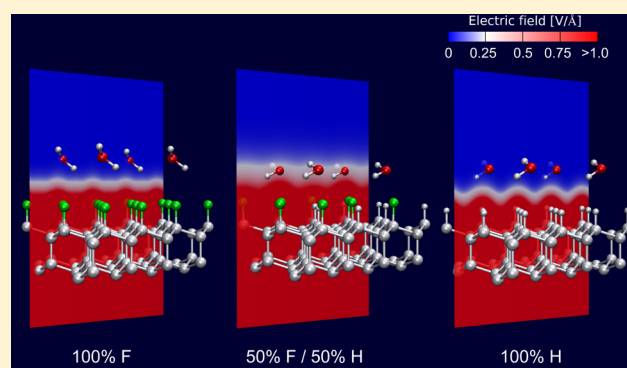
INTRODUCTION

Fluorination of carbon compounds is a key technique in chemistry, especially in the fields of biochemistry, pharmaceuticals, and materials science.[1−4] The usefulness of incorporating fluorine in organic molecules and carbon materials can, to a large extent, be traced back to the special properties of the C−F bond, which is highly polar and the strongest bond found in organic chemistry.[5] Moreover, the small size of the fluorine atom, whose 0.14 nm van der Waals radius is only slightly larger than the 0.12 nm radius of H, is a good precondition for the partial or complete substitution of C−H by C−F bonds.[3,6] In addition to the high stability and chemical inertness, fluorinated compounds usually show pronounced hydrophobicity that is exploited, for example, in medical applications and for the production of stain- and water-repellent surfaces.[7] The poor interaction of many fluorinated carbon materials with polar solvents is attributed to the C−F bond generally being a weak hydrogen bond acceptor despite its polar character.[5,6,8]

Empirically, only very few exceptions of strong C−F⋯H bonds have been found if the H⋯F hydrogen bond length is taken as a measure of the hydrogen bond strength.[9−11] In general, hydrogen bonds are considered strong when their binding energies exceed 0.2 eV, and the bond lengths are considerably shorter than the sum of the van der Waals radii of the involved elements.[12] However, intra-[13] and intermolecular[8,14,15] electrostatic interactions can be of high relevance in organofluorines. This apparent discrepancy between the polarity of the C−F bond and the hydrophobicity of many fluorinated carbon compounds has been termed as "polar hydrophobicity".[6] Hydrophobic behavior was not only found for molecular fluorocarbons but also for fluorinated diamond[16−18] and diamond-like carbon surfaces,[19] as well as for nanostructured carbon materials.[20] Consistently, it was found
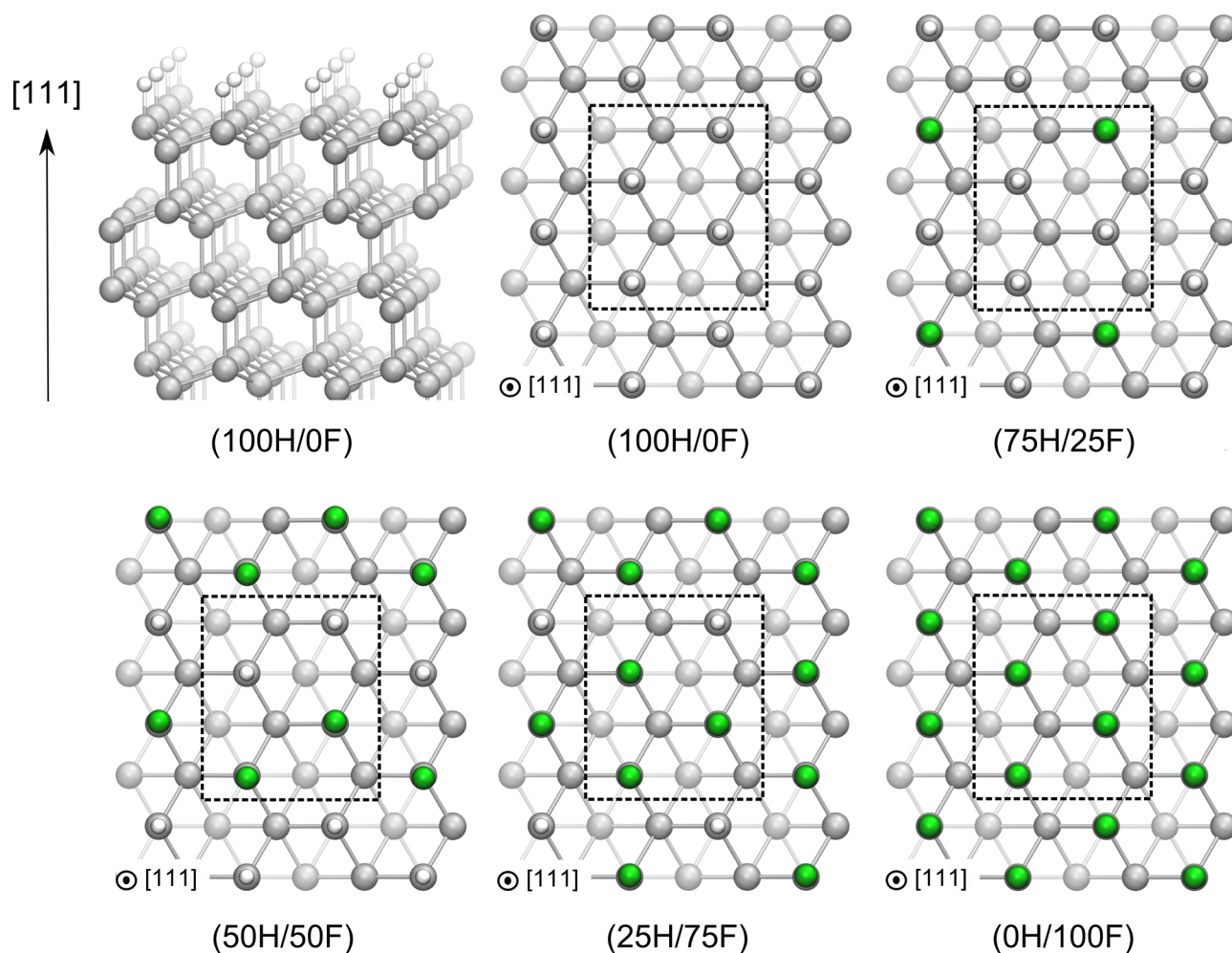
Figure 1. Geometries of the investigated F/H-terminated C(111) surfaces. The composition of the different surface terminations is denoted by the percentage of the surface covered by H and F atoms. Carbon atoms are depicted by gray, hydrogen by white and fluorine by green spheres. The surface unit cells are highlighted by dashed rectangles. The top-left panel shows a side view of the H-terminated C(111) system. Top views onto the (111) surface are shown in the other panels.

that self-assembled monolayers of fluorocarbons behave hydrophobically and the polarity of C−F bonds does not influence the interaction with water molecules in this case.[21,22] However, strong interactions between water and carbon surfaces were observed in density functional theory (DFT) and classical molecular dynamics (MD) simulations of partially F-terminated graphene[23] and diamond (111) surfaces[24] [C(111) surfaces] and of C(111) surfaces terminated by a mixed monolayer of Na and F atoms.[25]

Meng et al.[25] attribute the strong binding of water on Na/F-terminated diamond to a strong electrostatic bond between single partially ionized Na atoms and H_2O. However, the proposed interaction mechanism does not yield a universal description of the interaction of polar surfaces with water, since it obviously fails to explain polar hydrophobicity of perfluorinated carbon materials, where the surface polarity is due to partially ionized F instead of Na atoms.

In this paper, the mechanisms that lead to polar hydrophobicity of fully fluorinated carbon compounds as well as the hydrophilicity caused by a mixed F/H termination are worked out. For this purpose, the interaction of single H_2O molecules with fully hydrogenated, fully fluorinated, and mixed F/H-terminated C(111) surfaces is initially studied using ab initio DFT calculations. We find that the H_2O adsorption energy is

dominated by electrostatic contributions and exceeds 0.2 eV for the mixed F/H-terminated surfaces, while the adsorption is much weaker and mainly due to dispersion forces in the fully fluorinated and hydrogenated cases, which have adsorption energies of 0.07 and 0.09 eV, respectively. Hence, a transition from a weak to a strong hydrogen bond regime is observed. The results of the DFT calculations are rationalized by a simple model based on classical point charges, which is both able to account for and explain the high variation in adsorption energies and electrostatic contributions for the different surface terminations. The classical point-charge model allows the parametrization of a classical force field based on the optimized potentials for liquid simulations (OPLS),[26] which reproduces the adsorption energies of the single water molecule on the F/H-terminated C(111) surfaces and is used to simulate the contact angle of a water droplet on the same surfaces. The results of these MD simulations show a pronounced correlation between single-molecule adsorption energy and contact angle. Finally, we investigate the generality of the proposed model. The findings obtained for the solid diamond surfaces are transferable to molecular systems: partially fluorinated *n*-dodecanethiol molecules also exhibit a strongly enhanced electrostatic attraction to H_2O compared to their fully hydrogenated and perfluorinated counterparts. However, the

Table 1. Adsorption Energies (E_{ad}, in eV) and Hydrogen-Bond Lengths [$d(H_2O\cdots HC)$ and $d(HOH\cdots FC)$, in Å] for an Adsorbed H_2O Molecule on the C(111) Surfaces with Various Terminations. Bader Atom Charges of the Terminating F and H Atoms (q_F and q_H, in |e⁻|), and Bader Atom Charges of the H and O Atoms of the Adsorbed H_2O Molecule (q_{H,H_2O} and q_{O,H_2O}, in |e⁻|)[a]

	(100H/0F)	(75H/25F)	(50H/50F)	(25H/75F)	(0H/100F)
E_{ad}	0.09	0.23	0.23	0.23	0.07
$d(H_2O\cdots HC)$	2.63	2.45	2.29	2.16	
$d(HOH\cdots FC)$		1.95	2.24	2.36	2.44
q_F		−0.63	−0.62	−0.60	−0.59
q_H	−0.01	0.07	0.13	0.19	
q_{H,H_2O}	0.59	0.61	0.60	0.60	0.59
q_{O,H_2O}	−1.19	−1.21	−1.19	−1.17	−1.17

[a]For comparison, the Bader atom charges on an isolated H_2O molecule are −1.19 |e⁻| and 0.59 |e⁻| for the O and H atoms, respectively.

model cannot be used to describe all polar terminations and is limited to systems where the electron charge is localized and can be treated as a point charge, as shown by a comparison between F- and Li-terminated C(111) surfaces.

METHODS

DFT Simulations. The adsorption energies of single H_2O molecules on various F/H-terminated C(111) surfaces are determined by DFT as implemented in the Vienna ab initio Simulation Package (VASP).[27−29] Local and semilocal density functionals suffer from the absence of long-range correlation effects. Hence, while they account for correlation effects at short bonding distances rather well, they cannot describe long-range dispersion interactions, which are of special importance in otherwise weakly bound systems.[30,31] Therefore, in order to describe such systems with chemical accuracy, local and semilocal density functionals can only be employed if they are corrected such that they explicitly include long-range dispersion interactions. A convenient approach that is computationally efficient and has nevertheless proven to yield good accuracy is the so-called DFT-D method, where a classical semiempirical pair potential is added to standard DFT calculations.[31] Here, we employ the semilocal Perdew−Burke−Ernzerhof (PBE) exchange−correlation functional[32] as the DFT method in connection with Grimme's PBE-D2[33] correction. Additionally, all single H_2O adsorption energies were calculated by using similar correction terms of Tkatchenko and Scheffler[34,35] and without any dispersion correction for comparison (see the Supporting Information). A plane wave energy cutoff of 400 eV, a k-point sampling of 4 in the lateral directions, and Gaussian smearing with a width of 0.05 eV are applied. For relaxations a force threshold of 0.01 eV/Å is used. Adsorption energies are determined as $E_{ad} = E_{surf} + E_{H_2O} − E_{H_2O@surf}$, where $E_{H_2O@surf}$ is the ground-state energy of the surface with adsorbed water, while E_{surf} and E_{H_2O} are the ground-state energies of the isolated diamond surface and a water molecule, respectively. With this definition, larger adsorption energies mean stronger bonding. The (111) diamond surfaces are represented by laterally repeated rectangular $\sqrt{3} \times 2$ supercells (see Figure 1) forming slabs with 6 atomic layers and hence containing 48 carbon atoms. The lattice dimensions of 4.38×5.05 Å² were derived from the lattice constant of the DFT-relaxed bulk diamond structure whose value of 3.58 Å is close to the experimental[36] lattice constant of 3.57 Å. Surface terminations and adsorbed water molecules are applied symmetrically on both surfaces in order to suppress any errors arising from the periodic boundary conditions along the surface normal. At least 15 Å of vacuum separate the surface atoms of two adjacent slabs. Diamond surfaces with varying ratios of H and F terminations are studied. They are labeled by their H and F content. For example, the surface with 75% H and 25% F coverage is denoted by (75H/25F). In total, surfaces with the compositions (100H/0F), (75H/25F), (50H/50F), (25H/75F), and (0H/100F) are studied. The corresponding surface unit cells are shown in Figure 1.

Classical MD Simulations. We simulate the adsorption of water on C(111) surfaces using an all-atom force field, which is based on the OPLS potential.[26] The TIP3P model[37] is used to describe water. The atomic interactions in bulk diamond are treated with the parameters for hydrocarbons.[38] The diamond C−C bond length is 1.526 Å. The bond-stretching and angle-bending parameters are modified in order to closely reproduce the experimental values[39] of the diamond elastic constants, yielding 15.110 eV for the bond-stretching parameter and 4.192 eV for the angle-bending parameter. A comparison between the model and experimental elastic constants is presented in the Supporting Information. The H-terminated diamond surface is treated with the OPLS parameters for hydrocarbons,[38] while the parameters for perfluoroalkanes[40] are used for the F terminations. However, the electrostatic potential (ESP) atomic charges[41] from our DFT simulations instead of the original OPLS ones are used for H (0.09 |e⁻|, e⁻ = electron charge) and F (−0.20 |e⁻|). Moreover, the OPLS Lennard-Jones parameters σ_H and σ_F are shortened by about 18% (σ_H = 2.05 Å and σ_F = 2.40 Å) in order to obtain the DFT value for the adsorption energy (i.e., 0.23 eV) for the single water molecule on the (50H/50F) surface. This force field is used to calculate the contact angles for a 2000-molecule water droplet on a $112.22 \times 114.63 \times 12.21$ Å³ C(111) slab where periodic boundary conditions are applied along the two directions (x and y) parallel to the terminated surfaces. We consider the five different F/H surface terminations used in the DFT simulations. To measure the contact angle, we perform 2-ns-long MD simulations with a Langevin thermostat to keep the system at 300 K, and we calculate the contact angle during the last 1 ns simulation period with the method explained in the works of Werder et al.[42] and Sedlmeier et al.[43] For each surface termination, the geometry of the water droplet is determined by averaging the position of the Gibbs dividing surface over 100-ps-long periods, thus obtaining 10 values of the contact angle for each surface termination.

RESULTS AND DISCUSSION

DFT Calculations of H_2O Adsorption on F/H-Terminated C(111) Surfaces. In this work, the C(111) surface is used as a model system to explore the effect of fluorination on the interaction between a carbon surface and individual H_2O molecules. Due to the good substitutability of C−H by C−F bonds, surfaces with varying ratios of H and F coverage can be examined. In more detail, we start with the fully hydrogenated diamond surface and successively replace H by F until a fully fluorinated surface is obtained. By doing so, we obtain the five different F/H-terminated diamond surfaces, the unit cells of which are shown in Figure 1.

For the fully fluorinated and fully hydrogenated surfaces, maximal adsorption energies of 0.07 and 0.09 eV are found, respectively (see Table 1 and Figure 2). This is in agreement with the general expectation that the C−F bond has a very low polarizability and hence is a very weak hydrogen-bond acceptor, even if compared to the weak hydrogen-bond donor C−H.[8] More unexpected is the water adsorption at the mixed F/H-terminated surfaces. The interaction of these surfaces with H_2O
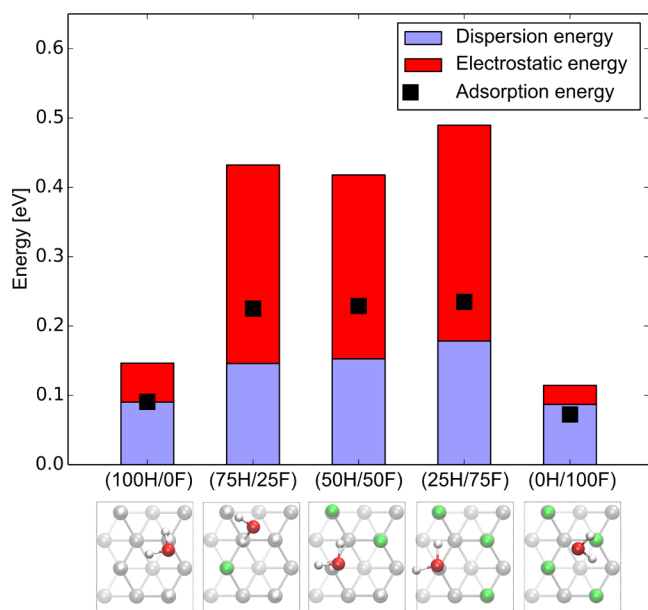
Figure 2. Adsorption energies (■) of a single H_2O molecule on the investigated C(111) surfaces with different F/H terminations as well as the electrostatic (red) and dispersion force (blue) contributions to the adsorption energies. Note that the sum of the attractive electrostatic and dispersion force contributions reproduces the trend in the adsorption energy, although the latter is smaller since it also includes the core−core repulsion. Top views of the H_2O adsorption geometries are shown at the bottom.

Figure 3. (a) Near-surface electric field strength for the investigated F/H-terminated C(111) surfaces. Here we show the electric field strengths in two-dimensional cross sections through the center of the O atom of the adsorbed H_2O molecules, which are displayed in their optimized adsorption positions. (b) Electric field strength averaged over the lateral directions along the surface normal z of the various investigated F/H-terminated C(111) surfaces. The highest surface atom of each surface has been used to define $z = 0$. The positions of the O atom from the adsorbed H_2O molecules are indicated by vertical dashed lines in order to indicate whether the H_2O molecules adsorb in regions of high or low fields. (c) Schematics showing the potential energy (solid lines) for a H_2O molecule approaching a surface with electric fields that have a shorter (S) or longer (L) range than the core−core repulsion. In the case of a long-range electric field there is a region, indicated by the red color, where the electrostatic attraction (dashed−dotted lines) outweighs the core−core repulsion (dashed lines), leading to an effective bonding of H_2O molecules due to electrostatics. In the case of short-range electric fields, bonding due to electrostatics is absent. For simplicity, the effect of the attractive dispersion interaction is neglected in the schematics. In parts a and b, we indicated whether the investigated surfaces are of type L or S.

is much stronger than in the pure H and F termination cases, resulting in an E_{ad} of 0.23 eV for all mixed surface terminations (see Table 1 and Figure 2). The optimized geometries of the adsorbed water molecules for the various surfaces are shown in Figure 2 and Figure 3a. We observed a clear trend of decreasing hydrogen bond length $d(H_2O\cdots HC)$ between the O atom of the water molecule and the closest H atom on the surface with decreasing H content [ranging from 2.63 Å for the (100H/0F) surface to 2.16 Å for the (25H/75F) surface]. Likewise, there is a decrease of the bond length $d(HOH\cdots FC)$ (between the H atom of water and the closest F atom on the surface) with decreasing F content [ranging from 2.44 Å for the (0H/100F) to 1.95 Å for the (75H/25F) surface; see Table 1]. Hence, it becomes apparent that decreasing the H content successively converts the remaining surface H atoms into stronger hydrogen-bond donors, and likewise, a decreasing F content converts the remaining surface F atoms into better hydrogen-bond acceptors. In order to elucidate the nature of the considerably enhanced interaction between the surface and H_2O for the mixed F/H-termination cases, both the electrostatic and dispersion contributions to the adsorption energy are extracted. The electrostatic contribution is determined as the electrostatic energy of the H_2O charge density immersed in the Hartree potential generated by the functionalized diamond surfaces (see the Supporting Information for more details). For this purpose, separate DFT simulations of the H_2O molecule and the diamond surfaces with atom positions from the relaxed adsorption geometries are carried out. The dispersion contributions were directly extracted from the D2 correction term. The results of this analysis are shown in Figure 2.

Interestingly, the electrostatic contribution dominates over the dispersion interaction for the mixed F/H-terminated surfaces, while there is only a very small electrostatic interaction
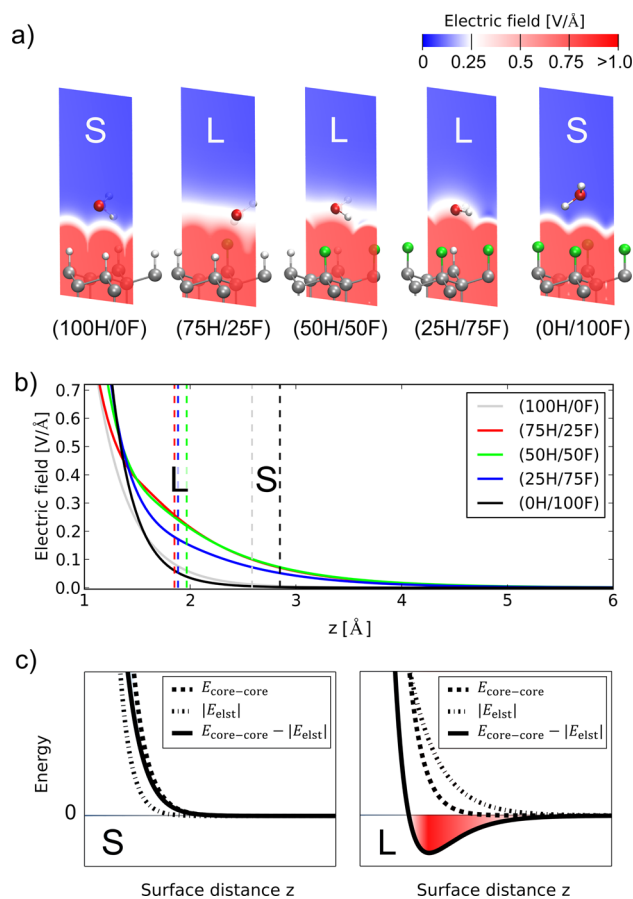
between H_2O and the fully hydrogenated and fluorinated surfaces. Moreover, the dispersion interaction is almost constant, while a pronounced variation in the electrostatic energy for the different surface terminations can be observed. The slightly enhanced dispersion contribution for the mixed surfaces can be traced back to the smaller adsorption bond lengths as a consequence of the increased electrostatic interaction. It is important to note that the sums of the attractive electrostatic and dispersion force contributions are not equal to the adsorption energies, since the latter additionally contain the core−core repulsion. Their strong electrostatic interaction suggests that the surfaces with mixed

terminations are highly polar. This conclusion is supported by the Bader charge analysis, which yields negative partial charges ranging between 0.60 and 0.63 electron charges ($-|e^-|$) on the F surface atoms (Table 1). A slight increase of the partial F charge with decreasing F coverage can be attributed to the H surface atoms donating some electron density to F atoms. This is consistent with the fact that the partial H atom charges become slightly positive and increase from $-0.01\ |e^-|$ to $+0.19\ |e^-|$ with increasing F content. A similar behavior was reported[44,45] for the successive substitution of H in CH_4 by F and for partially fluorinated diamond surfaces. Moreover, the Bader charges on the adsorbed water molecules are almost constant and coincide with the corresponding values of an isolated H_2O molecule, indicating that there is no charge transfer between adsorbed water and the C(111) surfaces. Although the high polarity of the mixed F/H-terminated diamond surfaces is necessary for a strong electrostatic interaction with H_2O, it is not sufficient to explain the strong H_2O adsorption.

The almost complete absence of electrostatic interactions in case of the (0H/100F) surface is puzzling, since also in this case a Bader charge of $-0.59\ |e^-|$ is located on the F surface atoms, again suggesting a highly polar surface. To resolve this seeming contradiction the near-surface electric field (NSEF) is analyzed for the various surfaces (Figure 3). Indeed, the NSEF exhibits a qualitatively different behavior for the different cases. Figure 3a displays the strength of the NSEF on vertical two-dimensional cross sections through the O atom of the adsorbed H_2O molecule. Water adsorbs in a region of enhanced NSEF on top of the mixed F/H-terminated surfaces only. This is in strong contrast to the fully H- and F-terminated surfaces that exhibit a fast decay of the NSEF. In this case, the field strengths averaged over the lateral directions decay along the surface normal (z direction) within 2 Å from the surface to values below $\sim$0.05 V/Å, whereas the decay for the mixed F/H-terminated surfaces is considerably slower (Figure 3b), resulting in a stronger electrostatic interaction with water.

Dipole Lattice Model for the Electric Field. To elucidate the origin of the different decay behaviors observed for pure and mixed fluorination, it is beneficial to take a look at simple lattice dipole models based on point charges. In the past, such models were used[46,47] to explain the interaction between polar surfaces and the range of electrostatic interactions at the surfaces of simple ionic crystals. Within these models, the electric field **E** is proportional to the surface dipole density, but most importantly, it decays exponentially along the z-direction. In leading order, the corresponding decay length is proportional to the lateral next-neighbor distance between the dipoles. More precisely, the electric field above a lattice of vertical dipoles formed by an upper plane of negative charges and a lower plane of positive charges, or vice versa, can be described by a rapidly converging series. Following the procedure of Lennard-Jones and Dent[47] and assuming that the point charges are located directly at the lattice points,

$$\mathbf{E} = \frac{\sigma}{2\varepsilon_0} \sum_{l,m\neq 0} \frac{e^{-|\mathbf{G}_{l,m}||z-z_{up}|} - e^{-|\mathbf{G}_{l,m}||z-z_{low}|}}{|\mathbf{G}_{l,m}|}$$
$$\times \begin{pmatrix} -\sin(\mathbf{G}_{l,m}\mathbf{r})G_{l,mx} \\ -\sin(\mathbf{G}_{l,m}\mathbf{r})G_{l,my} \\ +\cos(\mathbf{G}_{l,m}\mathbf{r})|G_{l,m}| \end{pmatrix} \quad (1)$$

is obtained. Here, σ is the average surface charge density of the upper plane and $\mathbf{G}_{l,m} = l\mathbf{b}_1 + m\mathbf{b}_2$ is the linear combination of the primitive reciprocal lattice vectors $\mathbf{b}_1$ and $\mathbf{b}_2$. The integer summation indices l and m range from $-\infty$ to $+\infty$ (excluding $l = m = 0$, since we are dealing with overall charge neutral systems). The positions of the upper and lower plane along the z direction are given by z_{up} and z_{low}, respectively. The behavior of the electric field along the z-direction is determined by the terms with the largest decay length, which is given by $\lambda_{max} = 1/|\mathbf{G}_{min}|$, where $|\mathbf{G}_{min}| = \min_{l,m} \mathbf{G}_{l,m}$ is the length of the shortest reciprocal lattice vector. In the case of a hexagonal lattice, the relevant decay length is given by $\sqrt{3}d/4\pi \approx 0.14d$, where d is the nearest-neighbor distance between two lattice points. Therefore, on a dense, homogeneous dipole lattice, a fast exponential electric field decay can be expected, regardless of the surface polarity (which just enters as a prefactor via σ).

If this decay occurs within a distance from the surface that is smaller than the range of the core–core repulsion between the surface and the adsorbate atoms, any electrostatic interaction is suppressed (see the schematics in Figure 3c). We propose and substantiate below that this picture can be applied to the pure H- and F-terminated diamond surfaces, where uniform lattices of vertical dipoles ↓ and ↑ are formed by highly polar C−F or less polar C−H bonds, respectively. For the mixed F/H-terminated surfaces, inhomogeneities in the form of ↑-dipoles (↓-dipoles) that point into the opposite direction of the C−F ↓ -dipoles (C−H ↑-dipoles) on the dense homogeneous lattice are introduced. Within this simple picture, the point-charge lattices for the mixed surfaces can be represented by a superposition of the lattice of the fully fluorinated surface and a different lattice representing the inhomogeneities (Figure 4). In
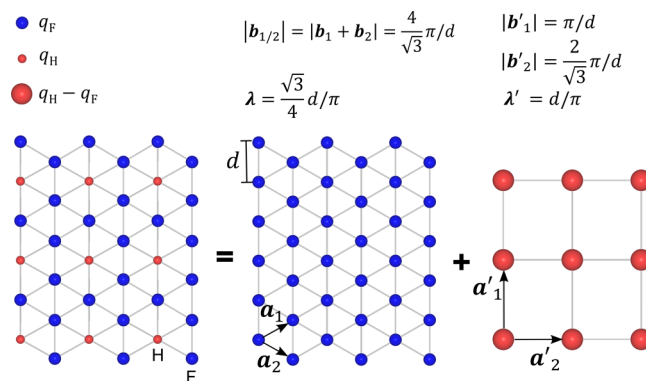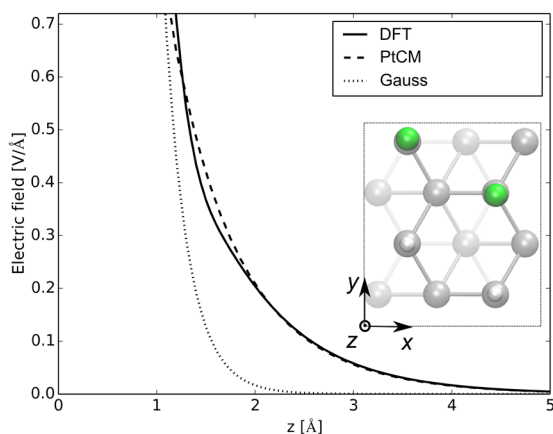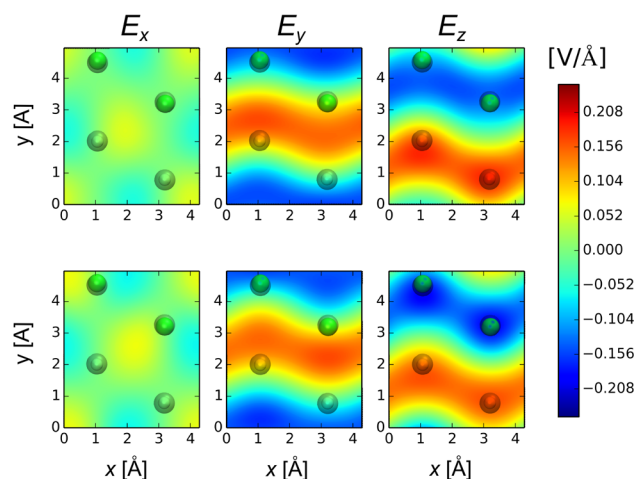

Figure 4. Scheme showing how the point-charge lattice representing the (25H/75F) C(111) surface (left) can be represented as the point-charge lattice of the purely F-terminated (0H/100F) surface (middle) and the lattice representing the difference between the (25H/75F) and the (0H/100F) point-charge lattices (right). Negative charges are shown as blue spheres; positive charges are shown as red spheres. The shortest reciprocal lattice vectors $\mathbf{G}_{min} = \pm\mathbf{b}_1, \pm\mathbf{b}_2, \pm(\mathbf{b}_1 + \mathbf{b}_2)$ of the dense hexagonal (0H/100F) lattice are much longer than the shortest reciprocal lattice vector $\mathbf{G}'_{min} = \pm\mathbf{b}'_1$ of the orthogonal right lattice, which describes the spatial distribution of the inhomogeneity introduced by the hydrogen atoms into the (25H/75F) lattice. Therefore, the inhomogeneity lattice at the very right side has a considerably larger electric field decay length $\lambda' = 1/|\mathbf{G}'_{min}|$ compared to the hexagonal (0H/100F) lattice and hence will govern the electric field behavior at the mixed (25H/75F) surface. We note that the point charges of the inhomogeneity lattice are given by $q_H - q_F$. Therefore, in this simple picture the near-surface electric field depends on the charge difference $q_H - q_F$ and not on the absolute values of q_H and q_F.
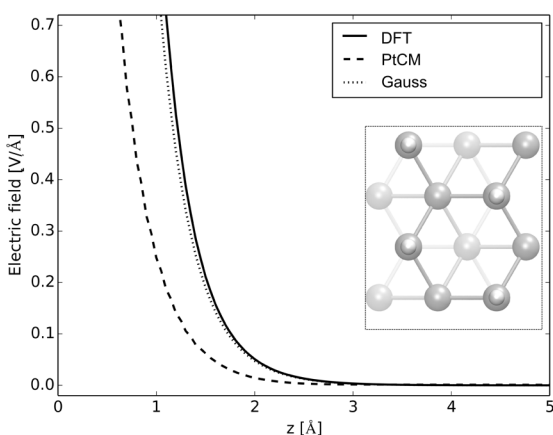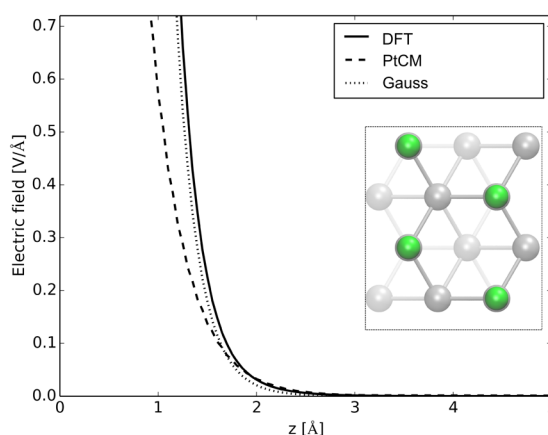
Figure 5. Averaged electric field strengths near the (50H/50H), (100H/0F), and (0H/100F) C(111) surfaces from DFT calculations (solid) and the fitted point-charge model (PtCM, dashed) and the contribution to the electric field due to the finite surface electron density according to Gauss's theorem (dotted). The insets show the unit cells of the surface model systems. For the (100H/0F) and (0H/100F) surfaces the near-surface electric field decays are mainly determined by the delocalized spill-out of electron density. Top right: E_x, E_y, and E_z components of the electric field in the x–y plane with a distance of $z = 2.2$ Å from the highest surface atom for the (50H/50F) surface. The electric field components as obtained from the DFT calculations are compared with the electric field components determined by the PtCM. The H and F atoms terminating the (50H/50F) surface are indicated. The plots of the averaged electric field strengths and of the E_x, E_y and E_z components for the (75H/25F) and (25H/75F) cases can be found in the Supporting Information.

the mixed surface termination cases considered here, the lattices of the inhomogeneities are less dense than the original lattice, leading to considerably smaller minimal reciprocal lattice vectors $|\mathbf{G}_{min}|$ and hence, according to eq 1, to longer decay lengths of the electric field. Applying this simple model to the investigated surfaces, a decay length of $\lambda_{mixed} = d/\pi \approx 0.32d$ is obtained for the mixed F/H-terminated surfaces in comparison to a much shorter decay length $\lambda_{fully\ F\ or\ H} = \sqrt{3}d/4\pi \approx 0.14d$ for the fully hydrogenated and fluorinated surfaces.

This estimate already suggests that for the mixed F/H-terminated diamond surfaces, the range of the electrostatic interactions can exceed the core−core repulsion range. Therefore, polar interactions can become relevant and even dominating. Thus, the electrostatic interaction between the surface and the H$_2$O molecule is not determined by the mere properties of single C−F or C−H bonds, but it is rather of nonlocal nature due to the superposition of C−F and C−H dipoles. As explained in Figure 4, the point charges assigned to the lattices representing the inhomogeneities are given by $\pm(q_H - q_F)$. Therefore, in the lattice model the near-surface electric

field mainly depends on the charge difference $q_H - q_F$ and not on the absolute values of q_H and q_F. This indicates that charge fluctuations relative to the charge on the F atoms cause the enhanced polarization of water at mixed F-terminated surfaces and not the absolute charge of the surface counterions (such as Na$^+$).[25]

Point-Charge Model versus Density Functional Theory. In order to check the applicability and the limits of the lattice model based on point charges in describing the near-surface electrostatic environment as determined by ab initio DFT calculations, we explicitly assign point charges q_H and q_F to the adsorbed H and F surface atoms and point charges $q_{C(H)}$ and $q_{C(F)}$ to the underlying next-neighbor C atoms. All charges are extracted from the best fit of this simple point-charge model (PtCM) to the NSEF from the DFT calculations. This is in the spirit of the electrostatic potential (ESP) charges often used in classical force fields.[41,48] The fitting is performed in a height range between 2 and 5 Å from the surface. Hereby the surface is defined as the z-coordinate of the highest surface atom. For simplicity, the constraint $q_{C(x)} = -q_x$ ($x = $ H, F) is introduced to

ensure overall charge neutrality. This assumption is verified by the Bader charge analysis, which gave negligible charges on the C atoms not directly bonded to F. The fitting procedure is applied to the NSEF of the (50H/50F) surface and the validity of the resulting PtCM is checked for the other investigated surfaces. We find that the electric field from the PtCM is rather insensitive to the absolute values of q_H and q_F but is mainly determined by the difference $q_H - q_F$, as predicted by the lattice models for the mixed F/H surface terminations (Figure 4). For this reason, q_F is fixed such that q_H remains the only free parameter to be fitted. We choose $q_F = -0.2$ |e⁻| as this value is within the range of partial charges used in well-established classical force fields that model fluorocarbons[22] or hydro-fluorocarbons.[49] The best fit is obtained for $q_H = 0.09$ |e⁻|. This is a typical value for the hydrogen charge in classical force fields for hydrocarbons.[26,49] Furthermore, the difference $q_H - q_F = 0.29$ |e⁻| is in good agreement with the classical force field model of Paulechka et al.[49] As shown in Figure 5 for the (50H/50F) surface [plots for the (75H/25F) and (25H/75F) cases are provided in the Supporting Information], in the mixed-termination cases both the decay of the averaged electric field strength along z as well as the spatial distribution of the single components of the electric field from the PtCM agree on a quantitative level with the corresponding DFT result for the mixed F/H terminated surfaces. In case of the pure (0H/100F) and (100H/0F) surfaces, the PtCM predicts an even faster NSEF decay than the DFT calculations.

This discrepancy can be traced back to the short-range spill-out of the DFT surface electron density in the vacuum. Due to this spill-out, close to the surface the overall system appears as effectively positively charged. According to Gauss's theorem, this leads to the generation of an additional electric field that is not included in the classical PtCM. In order to approximate the influence of the finite surface density, we first determine the electron density spill-out above a certain height z_0

$$Q(z_0) = \iint_A dA \int_{z_0}^{z_T} dz\, \rho(x,y,z),$$

where ρ is the DFT electron density, A is the area of the surface unit cell, and z_T denotes the top of the simulation box. Gauss's theorem is employed to estimate the averaged electric field upshift $E_{\text{Gauss},z}(z) = -Q(z)/\varepsilon_0 A$ due to the delocalized DFT surface electron density. Since the electric field decay as determined by DFT is practically identical to the Gauss's law estimate (see Figure 5), it can be concluded that the NSEF of fully H- and F-terminated surfaces is governed by the delocalized electron density spill-out, in contrast to the mixed F/H-terminated surfaces. In the latter case, $E_{\text{Gauss},z}(z)$ can be safely neglected for $z > 2$ Å, since in this region it is by far smaller than the slowly decaying field from the point charges (Figure 5). However, for all the considered surfaces, the NSEF behavior obtained by DFT is very similar to the PtCM prediction for $z > 2$ Å. In the Supporting Information, we provide a more detailed analysis of the electric field due to the electron spill-out at the (0H/100F) surface for the interested reader.

Molecular Dynamics Simulations of Water Droplets on F/H-Terminated C(111) Surfaces. The good agreement between the PtCM and DFT simulations on the electric field behavior suggests the parametrization of a classical force field, where the electrostatics is described by point charges, in order to study the relevance of the single-molecule adsorption energies on the wetting behavior of the surfaces. Previous

studies[42,50,51] showed that the adsorption energy of a single water molecule is highly correlated with the water contact angle on a specific surface. The TIP3P and an OPLS-based force field are used to describe water and F/H-terminated surfaces, respectively. In order to extend the DFT single-molecule results, we modify the original OPLS atomic charges and Lennard-Jones parameters of the H and F terminations so that the OPLS value of the adsorption energy for the single water molecule on the (50H/50F) surface matches the DFT value. These parameters are then used to calculate the adsorption energy for the other F/H-terminations (100H/0F), (75H/25F), (75H/25F), (0H/100F). The OPLS adsorption and Coulomb energies are reported in Table 2. Next, we calculate

Table 2. DFT and OPLS Adsorption Energies [E_{ad}(DFT) and E_{ad}(OPLS), in eV] and the Electrostatic Contributions [E_{elst}(OPLS), in eV] to E_{ad}(OPLS) for the Adsorption of a Single H₂O Molecule at the Differently Terminated C(111) Surfaces

termination	E_{ad}(DFT)	E_{ad}(OPLS)	E_{elst}(OPLS)
(100H/0F)	0.09	0.08	0.01
(75H/25F)	0.23	0.24	0.21
(50H/50F)	0.23	0.23	0.19
(25H/75F)	0.23	0.20	0.14
(0H/100F)	0.07	0.06	0.00

the contact angles for a 2000-molecule water droplet on a $112.22 \times 114.63 \times 12.21$ Å³ C(111) slab (the details about the simulations and the choice of parameters are provided in the Methods section).

Figure 6 shows the contact angles as well as the adsorption energies for the different F/H-terminations. We note that
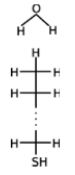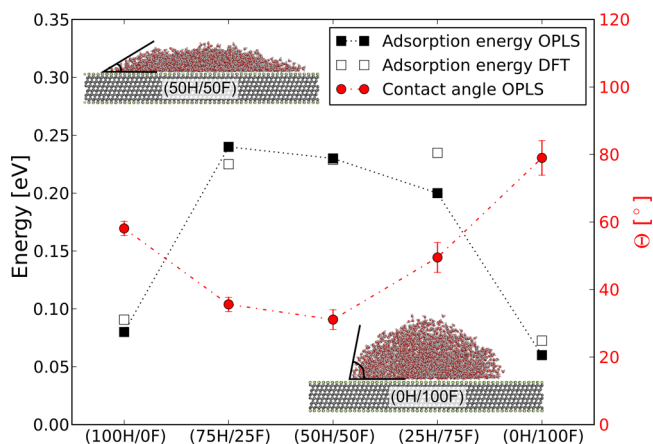
Figure 6. Adsorption energies of a single H₂O molecule determined by OPLS (filled squares) and DFT (open squares) and the contact angle (red circles) determined by OPLS MD simulations for the C(111) surfaces with different F/H terminations. The insets show snapshots taken from MD trajectories of water droplets on the (50H/50F) and (0H/100F) surfaces.

although the values of the contact angle are qualitative, the model clearly shows that the same trend followed by the adsorption energies as a function of the F/H coverage is also followed by the contact angle and, hence, emphasizes the importance of electrostatically dominated single-molecule adsorption energies for the macroscopic wetting behavior of the considered surfaces.

Generalization and Limits: Molecular Carbon Compounds and the Lithiated C(111) Surface. An interesting question for future studies is whether the fast decay of the electric field on fluorinated carbon surfaces and the enhanced electrostatic interaction for mixed F/H functionalizations can only be observed for extended planar dipole lattices as represented by the investigated fluorinated and hydrogenated C(111) surface or also holds for topologically distinct carbon structures, such as molecular carbon compounds. In order to explore this possibility, the adsorption energies of a H_2O molecule at the CH_3 and CF_3 terminations of n-dodecanethiol ($C_{12}H_{25}SH$) and n-perfluorododecanethiol ($C_{12}F_{25}SH$) are studied, respectively. These groups were used by Dalvi and Rossky[22] for their study of water adsorption on self-assembled monolayers. Additionally, one of the fluorine atoms of the CF_3 termination of the perfluorocarbon is replaced by a hydrogen atom (obtaining the stoichiometry $C_{12}F_{24}HSH$) introducing a perturbation into the regular dipole arrangement of the C–F bonds (in analogy to the approach used for the diamond surface). Likewise, one of the hydrogen atoms at the n-dodecanethiol CH_3 head is substituted by F (obtaining $C_{12}H_{24}FSH$).

The adsorption energies show the same trend as for the functionalized diamond surface. In the case of the fully fluorinated and hydrogenated molecules, relatively small adsorption energies of 0.05 and 0.06 eV are found, whereas the mixed cases show again strongly enhanced adsorption energies of 0.18 eV ($C_{12}F_{24}HSH$) and 0.21 eV ($C_{12}H_{24}FSH$), respectively. Again, the electrostatic and dispersion contributions to E_{ad} reveal that electrostatic contributions are reduced for the fully fluorinated and hydrogenated thiols, while they dominate water adsorption on $C_{12}F_{24}HSH$ and $C_{12}H_{24}FSH$ (see Table 3).

Table 3. Adsorption Energies (E_{ad}) and Dispersive as well as Electrostatic Contributions (E_{disp} and E_{elst}) to the Adsorption Energy for the Adsorption of a Single H_2O Molecule at the Head Group of n-Dodecanethiol $C_{12}H_{25}SH$ and the Therefrom Derived Partially Fluorinated or Perfluorinated Molecules $C_{12}H_{24}FSH$, $C_{12}F_{24}HSH$, and $C_{12}F_{25}SH$

	$C_{12}H_{25}SH$	$C_{12}H_{24}FSH$	$C_{12}F_{24}HSH$	$C_{12}F_{25}SH$
E_{ad}	0.06 eV	0.21 eV	0.18 eV	0.05 eV
E_{disp}	0.05 eV	0.05 eV	0.07 eV	0.05 eV
E_{elst}	0.05 eV	0.26 eV	0.25 eV	0.03 eV

Finally, we address the question whether electrostatic interactions are generally suppressed at surfaces that are homogeneously and densely terminated by polar functionalities. To do this, we consider the Li-terminated C(111) surface, where lithium has a positive partial atomic charge due to its very low electronegativity. This system is most likely prone to hydrolysis, but it can serve as a model system to illustrate the limits of simple classical force fields based on point charges in describing water at polar surfaces. In contrast to H and F, Li adsorbs at a hollow-type position on top of the second highest C atoms, as shown in Figure 7a. The DFT adsorption energy E_{ad} of H_2O on the fully Li-terminated surface is 0.52 eV, considerably larger than E_{ad} on the F/H-terminated surfaces. In contrast to the fully fluorinated and hydrogenated surfaces, the electrostatic contribution of 2.09 eV to E_{ad} dominates over the dispersion force contribution of 0.32 eV. This is consistent with the NSEF that decays much more slowly than for the F/H surface terminations (see Figure 7b) such that water adsorbs in a region of high electric field, as shown in Figure 7a.

In order to understand the origin of the long-range NSEF, the PtCM contribution to the electric field (see the Supporting Information for details) is compared to the contribution from electron spill-out (estimated by Gauss's theorem and the DFT electron density). Figure 7b shows that the PtCM electric field decays significantly faster than the DFT electric field, while the NSEF determined from Gauss's theorem reproduces the DFT result very well. As a result, the slow NSEF decay can be attributed to the spill-out of surface electron-density. In comparison with the fully fluorinated and hydrogenated surfaces, the electron density of the fully lithiated surface extends much further into the vacuum (Figure 7c). Therefore, the Gauss field due to the electron density spill-out decays much more slowly than in the F/H-terminated cases. This results in a strong electric field for distances >2 Å from the surface (Figure 7b). Consequently, the adsorbed water experiences a sizable NSEF (Figure 7a). In summary, Li- and F-terminated C(111) surfaces exhibit very different electron spill-outs due to different adsorption configurations (see the Supporting Information). Despite F's strong electronegativity, the charge remains strongly localized on the C–F bonds, while it is delocalized on Li-terminated C(111) surfaces. In the latter case, point-charge models are not suitable to properly describe the electrostatic environment near the surface.

■ CONCLUSIONS AND OUTLOOK

The interaction between a diamond surface and a water molecule leads to strong hydrogen bonding for mixed F/H terminations, whereas for fully hydrogenated or fluorinated surfaces, the surface water interaction is considerably reduced. The reason for the qualitatively different behaviors is related to the near-surface electric field that decays extremely fast for the fully hydrogenated surface and even for the highly polar fully fluorinated surface. Surprisingly, the field decay is much slower for the mixed F/H terminations.

A simple point-charge model is able to reproduce the electrostatic trends obtained by the DFT calculations. Within this model the varying decay lengths for the different surface terminations result from the superposition of surface dipoles residing on 2D lattices with different densities. A dense and homogeneous dipole lattice (representative for fully hydrogenated or fluorinated surfaces) results in a very fast decay of the near-surface electric field and a strongly reduced electrostatic interaction with water, irrespective of the surface polarity. Thus, the fully fluorinated C(111) surface represents an example where the origin of polar hydrophobicity can be understood. On the other hand, the mixed F/H-terminated surfaces are represented by a superposition of the dense and homogeneous dipole lattice of a fully F- or H-terminated system and a dilute lattice with opposite dipoles for the introduced inhomogeneities. Due to the slow electric field
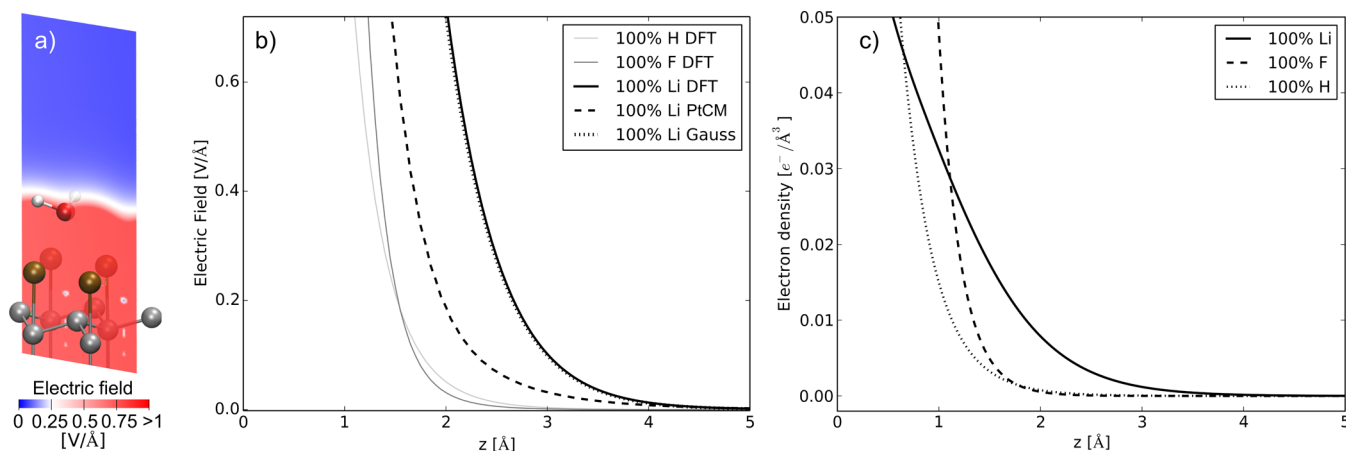
Figure 7. (a) Structure of the fully Li-terminated C(111) surface with an adsorbed water molecule. The near-surface electric field strength is shown in a plane through the O atom of the H_2O molecule. (b) Averaged electric field strength along the surface normal z of the purely Li-terminated (solid black), F-terminated (solid gray), and H-terminated (solid light gray) surfaces. For comparison, the electric field strength from the PtCM for the fully lithiated surface with a point charge of 1.0 $|e^-|$ (see the Supporting Information) on the Li ions (dashed) and the electric field strength due to the finite surface electron density according to Gauss's theorem (dotted) are shown. (c) Averaged surface electron density along the surface normal for the fully Li-terminated (solid), F-terminated (dashed), and H-terminated (dotted) diamond surfaces. For parts b and c, the z-coordinate of the highest atom of each surface has been used to define $z = 0$.

decay of the dilute lattice, the range of the surface electric field exceeds the range of the core–core repulsion between surface atoms and the adsorbed water molecule. Therefore, electrostatic interactions become strong enough to induce pronounced hydrogen bonding between mixed F/H-terminated surfaces and water molecules.

The good agreement between DFT calculations and a simple point-charge model on the behavior of the near-surface electric field enables the use of classical force fields to extend the single-molecule results to MD simulations where water droplets on surfaces are considered. MD simulations performed with a reparametrized OPLS potential and 2000-molecule water droplets show that the increased interaction between the mixed F/H-terminated surfaces and water on a molecular level is also effective in this more macroscopic scenario and leads to considerably decreased contact angles with respect to the completely hydrogenated and fluorinated cases. The latter surface is the most hydrophobic one, as already expected from the single-molecule results.

Additional DFT calculations of H_2O adsorption on partially fluorinated and perfluorinated *n*-dodecanethiols show that suppression and enhancement of electrostatic interactions at perfluorinated and partially fluorinated carbon structures are not restricted to planar, infinite, solid surfaces but can already be of relevance for smaller, finite accumulations of dipoles, such as in molecular compounds. This finding can, for example, explain the absence of any effect due to the polarity of C–H and C–F bonds in the works of Mezger et al.[21] and Dalvi and Rossky[22] on the interaction of water with fully fluorinated and hydrogenated SAMs. Future investigations that apply a combination of ab initio methods and dipole and point-charge models to molecular perfluorinated or partially fluorinated hydrocarbons will be fruitful to gain a deeper understanding of polar hydrophobicity.

Our results show that the decay behavior of the near-surface electric field is a crucial quantity to understand and describe the electrostatic interaction between polar substrates and polar molecules. In certain cases, such as the fluorinated and hydrogenated diamond surfaces, classical force fields that incorporate electrostatic interactions via point charges can be

successfully applied to qualitatively and, with some limitations, also quantitatively predict the behavior of polar surfaces. However, point-charge models can fail when surface charge density spills out toward the water adsorption site, as we have shown for the Li-terminated C(111) surface. Hence, in general, care must be taken when modeling polar surfaces using classical point-charge models and the near-surface electric field should be compared with ab initio electronic structure calculations for suited test systems beforehand.

In order to verify the theoretical predictions, direct experimental measurements of near-surface electric fields or potentials would be desirable. Possible experimental techniques that might be appropriate to tackle this task in the future are electron holographic tomography[52,53] or the recently developed[54] scanning quantum dot microscopy. On the theoretical side, first preliminary results indicate that the influence of near-surface electric fields on the contact angles can be reliably predicted by combining the Young–Lippmann equation[55] with ab initio calculations of the near-surface electric fields and with adequate polarizable continuum models[56] for water. With this method, a fast prediction of the role of electrostatic interactions on polar surfaces might become possible. An interesting application could be, for example, the investigation of OH-terminated surfaces.[43,57]

■ ASSOCIATED CONTENT

⑤ Supporting Information

The Supporting Information is available free of charge on the ACS Publications website at DOI: 10.1021/jacs.5b04073.

Bulk elastic constants of diamond, electrostatic potential profiles, calculation of the electrostatic contribution to the adsorption energy of H_2O, adsorption energies of single H_2O molecules on F/H-terminated C(111) surfaces, adsorption energies of single H_2O molecules on F/H-terminated C(111) surfaces, comparison of the electric fields determined by density functional calculations and by the point-charge model fitted to the DFT results, estimation of the contribution from the electron density spill-out to the near-surface electric field,

adsorption energy of a *Ih* ice bilayer on F/H-terminated C(111) surfaces, and analysis of the electron spill-out on the fully lithiated C(111) surface (PDF)

■ AUTHOR INFORMATION

Corresponding Authors
*leonhard.mayrhofer@iwm.fraunhofer.de
*srinivasan.rajagopalan@exxonmobil.com

Notes
The authors declare no competing financial interest.

■ REFERENCES

(1) *Organofluorine Compounds: Chemistry and Applications*; Yamamoto, H., Ed.; Springer-Verlag: Berlin, 2000.
(2) Chambers, R. D. *Fluorine in Organic Chemistry*; Blackwell Publishing Ltd: Oxford, 2004.
(3) Siegemund, G.; Schwertfeger, W.; Feiring, A.; Smart, B.; Behr, F.; Vogel, H.; McKusick, B. *Ullmann's Encyclopedia of Industrial Chemistry*; Wiley: New York, 2012; pp 443−494.
(4) Wang, J.; Sánchez-Roselló, M.; Aceña, J. L.; Del Pozo, C.; Sorochinsky, A. E.; Fustero, S.; Soloshonok, V. A.; Liu, H. *Chem. Rev.* **2014**, *114*, 2432−2506.
(5) O'Hagan, D. *Chem. Soc. Rev.* **2008**, *37*, 308−319.
(6) Biffinger, J. C.; Kim, H. W.; DiMagno, S. G. *ChemBioChem* **2004**, *5*, 622−627.
(7) Kissa, E. *Fluorinated Surfactants and Repellents*; Marcel Dekker: New York, 2001.
(8) Hyla-Kryspin, I.; Haufe, G.; Grimme, S. *Chem. - Eur. J.* **2004**, *10*, 3411−3422.
(9) Shimoni, L.; Glusker, J. P. *Struct. Chem.* **1994**, *5*, 383−397.
(10) Howard, J. A. K.; Hoy, V. J.; O'Hagan, D.; Smith, G. T. *Tetrahedron* **1996**, *52* (38), 12613−12622.
(11) Dunitz, J.; Taylor, R. *Chem. - Eur. J.* **1997**, *3*, 89−98.
(12) Desiraju, G. R. *Acc. Chem. Res.* **2002**, *35*, 565−573.
(13) Gooseman, N. E. J.; O'Hagan, D.; Peach, M. J. G.; Slawin, A. M. Z.; Tozer, D. J.; Young, R. J. *Angew. Chem., Int. Ed.* **2007**, *46*, 5904−5908.
(14) Dalvit, C.; Invernizzi, C.; Vulpetti, A. *Chem. - Eur. J.* **2014**, *20* (35), 11058−11068.
(15) Murray, J. S.; Ranganathan, S.; Politzer, P. *J. Org. Chem.* **1991**, *56*, 3734−3737.
(16) *CVD Diamond for Electronic Devices and Sensors*; Sussmann, R. S., Ed.; John Wiley & Sons: Chicester, UK, 2009.
(17) Salvadori, M. C.; Araújo, W. W. R.; Teixeira, F. S.; Cattani, M.; Pasquarelli, A.; Oks, E. M.; Brown, I. G. *Diamond Relat. Mater.* **2010**, *19*, 324−328.
(18) Nakamura, T.; Ohana, T.; Hasegawa, M.; Tsugawa, K.; Suzuki, M.; Ishihara, M.; Tanaka, A.; Koga, Y. *New Diamond Front. Carbon Technol.* **2005**, *16* (6), 313−324.
(19) Popov, C.; Kulisch, W.; Bliznakov, S.; Ceccone, G.; Gilliland, D.; Sirghi, L.; Rossi, F. *Diamond Relat. Mater.* **2008**, *17*, 1229−1234.
(20) Pastine, S. J.; Okawa, D.; Kessler, B.; Rolandi, M.; Llorente, M.; Zettl, A.; Fréchet, J. M. J. *J. Am. Chem. Soc.* **2008**, *130*, 4238−4239.

(21) Mezger, M.; Sedlmeier, F.; Horinek, D.; Reichert, H.; Pontoni, D.; Dosch, H. *J. Am. Chem. Soc.* **2010**, *132*, 6735−6741.
(22) Dalvi, V. H.; Rossky, P. J. *Proc. Natl. Acad. Sci. U. S. A.* **2010**, *107* (31), 13603−13607.
(23) Wang, P.; Wang, H.; Yang, W. *Phys. Chem. Chem. Phys.* **2014**, *16* (38), 20464−20470.
(24) Borisenko, K. B.; Reavy, H. J.; Zhao, Q.; Abel, E. W. *J. Biomed. Mater. Res., Part A* **2008**, *86A*, 1113−1121.
(25) Meng, S.; Zhang, Z.; Kaxiras, E. *Phys. Rev. Lett.* **2006**, *97*, 036107.
(26) Jorgensen, W. L.; Maxwell, D. S.; Tirado-Rives, J. *J. Am. Chem. Soc.* **1996**, *118*, 11225−11236.
(27) Kresse, G.; Furthmüller, J. *Phys. Rev. B: Condens. Matter Mater. Phys.* **1996**, *54* (16), 11169−11186.
(28) Kresse, G.; Joubert, D. *Phys. Rev. B: Condens. Matter Mater. Phys.* **1999**, *59* (3), 1758−1775.
(29) Blöchl, P. E. *Phys. Rev. B: Condens. Matter Mater. Phys.* **1994**, *50* (24), 17953−17979.
(30) Jones, R. O. *Rev. Mod. Phys.* **2015**, *87* (3), 897−923.
(31) Grimme, S. *Wiley Interdiscip. Rev. Comput. Mol. Sci.* **2011**, *1* (2), 211−228.
(32) Perdew, J. P.; Burke, K.; Ernzerhof, M. *Phys. Rev. Lett.* **1996**, *77*, 3865.
(33) Grimme, S. *J. Comput. Chem.* **2006**, *27*, 1787−1799.
(34) Tkatchenko, A.; Scheffler, M. *Phys. Rev. Lett.* **2009**, *102* (7), 073005.
(35) Tkatchenko, A.; DiStasio, R. A.; Car, R.; Scheffler, M. *Phys. Rev. Lett.* **2012**, *108* (23), 236402.
(36) *Handbook of Chemistry and Physics*, 89th ed.; Lide, D. R., Ed.; CRC Press: Boca Raton, FL, 2008.
(37) Jorgensen, W. L.; Chandrasekhar, J.; Madura, J. D.; Impey, R. W.; Klein, M. L. *J. Chem. Phys.* **1983**, *79* (2), 926.
(38) Jorgensen, W. L.; Maxwell, D. S.; Tirado-rives, J. *J. Am. Chem. Soc.* **1996**, *118*, 11225−11236.
(39) Zouboulis, E.; Grimsditch, M.; Ramdas, A.; Rodriguez, S. *Phys. Rev. B: Condens. Matter Mater. Phys.* **1998**, *57*, 2889−2896.
(40) Watkins, E. K.; Jorgensen, W. L. *J. Phys. Chem. A* **2001**, *105* (16), 4118−4125.
(41) Singh, U. C.; Kollman, P. A. *J. Comput. Chem.* **1984**, *5*, 129−145.
(42) Werder, T.; Walther, J. H.; Jaffe, R. L.; Halicioglu, T.; Koumoutsakos, P. *J. Phys. Chem. B* **2003**, *107*, 1345−1352.
(43) Sedlmeier, F.; Janecek, J.; Sendner, C.; Bocquet, L.; Netz, R. R.; Horinek, D. *Biointerphases* **2008**, *3* (3), FC23−C39.
(44) Wiberg, K. B.; Rablen, P. R. *J. Am. Chem. Soc.* **1993**, *115*, 614−625.
(45) Sen, F. G.; Qi, Y.; Alpas, A. T. *J. Mater. Res.* **2009**, *24*, 2461−2470.
(46) Israelachvili, J. *Intermolecular and Surface Forces*; Academic Press: London, 1991.
(47) Lennard-Jones, J. E.; Dent, B. M. *Trans. Faraday Soc.* **1928**, *24*, 92−108.
(48) Butenuth, A.; Moras, G.; Schneider, J.; Koleini, M.; Köppen, S.; Meißner, R.; Wright, L. B.; Walsh, T. R.; Ciacchi, L. C. *Phys. Status Solidi B* **2012**, *249*, 292−305.
(49) Paulechka, E.; Kroenlein, K.; Kazakov, A.; Frenkel, M. *J. Phys. Chem. B* **2012**, *116*, 14389−14397.
(50) Lange, B.; Posner, R.; Pohl, K.; Thierfelder, C.; Grundmeier, G.; Blankenburg, S.; Schmidt, W. G. *Surf. Sci.* **2009**, *603* (1), 60−64.
(51) Rafiee, J.; Mi, X.; Gullapalli, H.; Thomas, A. V.; Yavari, F.; Shi, Y.; Ajayan, P. M.; Koratkar, N. a. *Nat. Mater.* **2012**, *11* (3), 217−222.
(52) Wolf, D.; Lubk, A.; Röder, F.; Lichte, H. *Curr. Opin. Solid State Mater. Sci.* **2013**, *17* (3), 126−134.
(53) Sellner, B.; Kathmann, S. M. *J. Chem. Phys.* **2014**, *141* (18), 18C534.
(54) Wagner, C.; Green, M. F. B.; Leinen, P.; Deilmann, T.; Krüger, P.; Rohlfing, M.; Temirov, R.; Tautz, F. S. *Phys. Rev. Lett.* **2015**, *115* (July), 026101.

(55) Mugele, F.; Baret, J.-C. *J. Phys.: Condens. Matter* **2005**, *17* (28), R705−R774.

(56) Held, A.; Walter, M. *J. Chem. Phys.* **2014**, *141* (17), 174108.

(57) Janecek, J.; Netz, R. R. *Langmuir* **2007**, *23* (26), 8417−8429.